

RESEARCH ARTICLE

Demonstration of no catalytical activity of Fe-N-C and Nb-N-C electrocatalysts toward nitrogen reduction using in-line quantification

Arnar Sveinbjörnsson¹ | Anna Bergljót Gunnarsdóttir² | Erin B. Creel³ |
Camila Pía Canales² | Barr Zulevi⁴ | Xiang Lyu³ | Charl J. Jafta³  |
Egill Skúlason^{1,2,5} | Alexey Serov³  | Helga Dögg Flosadóttir^{1,2}

¹Atmonia ehf., Reykjavík, Iceland

²Faculty of Industrial Engineering, Mechanical Engineering and Computer Science, University of Iceland, VR-III, Reykjavík, Iceland

³Electrification and Energy Infrastructures Division, Oak Ridge National Laboratory, Oak Ridge, Tennessee, USA

⁴Pajarito Powder, LLC (PPC), Albuquerque, New Mexico, USA

⁵Science Institute, University of Iceland, VR-III, Reykjavík, Iceland

Correspondence

Helga Dögg Flosadóttir, Atmonia ehf., Keldnaholt, Reykjavík 112, Iceland.
Email: helgadogg@atmonia.com

Alexey Serov, Electrification and Energy Infrastructures Division, Oak Ridge National Laboratory, Oak Ridge, TN 37831, USA.
Email: serova@ornl.gov

Funding information

Icelandic Research Fund, Grant/Award Number: 196437-051; Icelandic Technology Development Fund, Grant/Award Number: 175350-0611; Icelandic Research Fund, Grant/Award Number: 1515-151377

Abstract

Ammonia (NH₃) production via the electrochemical nitrogen reduction reaction (NRR) is a promising method for sustainable generation of this important chemical. Efforts are ongoing in finding an efficient, stable, and selective catalyst that will enable the reaction. However, progress is hindered in the field due to lack of reproducibility, most likely a consequence of reports of false-positive results due to improper measurement control and methods. In this study, we explore the NRR activity of a promising class of single atom catalysts, transition metal-nitrogen-carbon (M-N-C) electrocatalysts. Using a state-of-the-art in-line ammonia quantification methodology, with detection limit as low as 1 ppb for ammonia, we show that single atom Nb and Fe embedded in a stable carbon and nitrogen framework do not electrochemically reduce N₂ to NH₃. Critically, this demonstrates that our experimental setup with in-line sequential injection analysis successfully excludes ammonia contamination from the gas supply and atmospheric sources, allowing for thorough and high-throughput examination of potential NRR catalysts.

KEYWORDS

ammonia synthesis, electrocatalysis, nitrogen electroreduction, NRR, single atom catalyst

This is an open access article under the terms of the [Creative Commons Attribution](https://creativecommons.org/licenses/by/4.0/) License, which permits use, distribution and reproduction in any medium, provided the original work is properly cited.

© 2022 The Authors. *SusMat* published by Sichuan University and John Wiley & Sons Australia, Ltd.

1 | INTRODUCTION

Ammonia (NH₃) is a promising clean energy carrier due to high energy density and high gravimetric hydrogen content. Additionally, it is one of the most produced chemicals worldwide and is critically important in the agriculture industry as a fertilizer.^{1–3} Ammonia is primarily produced via the Haber–Bosch process from nitrogen (N₂) and hydrogen (H₂) via Equation (1):^{4–7}



The Haber–Bosch process requires a large capital investment, is responsible for around 2% of global energy consumption, and is accompanied by around two tons of CO₂ emissions for each ton of ammonia produced.^{8–10} Thus, it is crucial to develop a green and versatile process for NH₃ synthesis from N₂.

Toward this aim, the electrochemical processes of reducing N₂ in aqueous solution is an attractive approach due to near-ambient operating conditions and the ability to use water as a sustainable hydrogen source.^{11–14} However, this reaction suffers from the low selectivity as it competes with the relatively facile hydrogen evolution reaction (HER), which results in low NH₃ reaction rates and low Faradaic efficiencies due to the stronger adsorption of protons than nitrogen atoms on the catalyst surface.¹⁵ Current research studies focus on how to suppress HER and simultaneously promote nitrogen reduction reaction (NRR), where tailoring the catalyst surface is the most common strategy to influence and steer activity and selectivity.

To improve the selectivity toward NRR, implementing electrolytes with low proton concentration, such as non-aqueous electrolytes,^{16,17} may be necessary and to date, the only process proven to produce ammonia electrochemically at high rates (30 nmol s^{−1} cm^{−2}) and efficiencies is the lithium-mediated NRR.^{18,19} In contrast, low yields of NH₃ are reported in most aqueous NRR studies (yield rates typically below 1 nmol s^{−1} cm^{−2}),²⁰ where quantification of NH₃ often relies on the highly sensitive colorimetric indophenol blue method or turbidimetric Nessler's method.^{21,22} Aqueous studies are still of significant interest albeit the low concentration makes it challenging to quantify ammonia in a reliable and reproducible manner. Furthermore, the field is plagued by false-positive results and researchers are calling for a more standardized and strict quantification methodology to improve reproducibility.^{18,20,23} False-positive results may arise from inadvertent nitrogen contamination sources in the environment, such as from the catalyst material, the N₂ gas stock, the electrolyte, and the electrochemical cell components, making it difficult to verify the electrosynthesis of NH₃.^{24–27}

Here, we follow a rigorous protocol for ammonia synthesis and quantification, using an in-line ammonia detection method previously reported by the authors.²⁸ In short, the sequential injection analysis (SIA) method uses an orthophthalaldehyde (OPA) reagent that reacts with ammonia to form a fluorescent compound, detected by a photomultiplier tube (PMT).²⁶ The advantages of the method are its high sensitivity and low salt effect, and for that reason, the method was developed to determine ammonium in seawaters.^{29,30} Furthermore, SIA is highly suitable for NRR studies; it is a commercial instrument that can easily be connected to an electrochemical cell where automated syringes are used to inject ammonia samples into the flowing carrier solution, where it mixes with the reagents before reaching the PMT detector. The electrolyte is contained in a gas tight environment and never exposed to atmosphere or handled in any manner. This minimizes external sources of contamination in samples providing a reproducible and reliable method to study NRR. The method only requires 200 μl volume of sample and has a detection limit as low as 1 ppb for ammonia, which allows for thorough and high-throughput screening of potential NRR electrocatalysts.³¹

Single atom catalysts (SACs) are a family of nanoengineered materials that contain atomically dispersed active sites embedded in a conducting framework, such as MoS₂, graphene, diyene, and nitrogen-doped carbon.³² SACs are attractive electrocatalytic materials due to low cost, diverse strategies of preparation and fabrication, and unique catalytic activity. Carbon-based SAC materials have shown good performance for various electrocatalytic processes, including the oxygen reduction reaction (ORR)^{33–35} and CO₂ reduction reaction (CO₂RR).^{36–38} Transition metal-nitrogen-carbon (M-N-C) catalysts are studied as potential catalysts to replace the platinum group metal-based catalysts in polymer electrolyte fuel cells, where Fe-N-C is considered the most promising alternative due to its high activity and selectivity toward ORR.^{39–41} M-N-C catalysts incorporate single atoms of metal catalysts into a carbonaceous matrix with N-doped sites.^{42,43} Furthermore, M-N-C electrocatalysts have been tested toward CO₂ reduction in neutral media.⁴⁴

As NRR catalysts, SACs have been investigated both experimentally and theoretically.⁴⁵ Choi et al. performed density functional theory (DFT) calculations on SACs that indicate suppression of HER with increased selectivity toward NRR.⁴⁶ Niu et al. screened SACs supported on graphitic carbon nitrides with DFT and predicted good catalytic activity and selectivity toward NRR of single atom Nb, Mo, Ta, and W.⁴⁷ Li et al. demonstrated Fe-based SAC on MoS₂ sheets as promising candidate with NRR reaction rate close to 36 mmol g^{−1} h^{−1}, which they attributed to high polarization at single atom protrusions.⁴⁸

In this work, potentially promising single atom M-N-C catalysts with Fe and Nb embedded in a carbon-nitrogen framework are evaluated for their electroactivity toward NRR as well as their electrochemical stability over time. We show that the two M-N-C materials, Fe-N-C and Nb-N-C, do not exhibit NRR activity toward NH_3 under the reaction conditions reported here. It is of great importance to report negative results of NRR catalysts since poor repeatability and numerous reports of false-positive results plague the scientific literature of electrochemical ammonia production. The negative result shown here in addition to previously positive NRR results reported by the authors²⁵ gives confidence in the in-line SIA quantification as a reliable method to definitively determine whether NRR to NH_3 has occurred.

2 | EXPERIMENTAL METHODS

2.1 | Materials

The following chemicals were used to prepare solutions and electrolytes in this study: KOH (Merck, $\geq 85\%$), NaOH (Honeywell Fluka, $> 98\%$), KCl (Supelco, for analysis), H_2SO_4 (Sigma Aldrich, 95–98%), and H_2O_2 (Sigma Aldrich, $> 30\%$). Gases were provided by Linde, N_2 (HiQ[®] Nitrogen 5.0) and Ar (HiQ[®] Argon 5.0). Orthophthalaldehyde (OPA, TCI, $> 99\%$) Nafion[™] 211 (Fuel Cell Store) membranes were prepared according to the protocol previously reported.²⁸ Ultra-pure water (MilliQ[®], Grade 1) was used in preparation of each solution.

2.2 | Preparation of M-N-C powder

The catalyst materials were synthesized by modified hard templating method as described in an earlier publication and practiced at Pajarito Powder, LLC as a VariPore[™] method.⁴⁹ Fe-N-C and Nb-N-C powders were prepared by the following procedure: The metal precursor, that is, 2.5 g iron nitrate nonahydrate (Sigma Aldrich, 98%) or 2.5 g ammonium niobate(V) oxalate hydrate (CBMM, 99%) respectively, was mixed with 25 g of Pipemidic acid (Sigma Aldrich, 98%) and 10 g of LM-150 fumed silica (Cabot Cab-O-Sil[®]) in 100 ml of deionized water (DI) water. The mixture was stirred for 2 h, and water was evaporated at 85°C in air. The obtained powder was ground with mortar and pestle and heat treated in tube furnace using Ultra High Purity (UHP) nitrogen at 980°C for 75 min at 100 ml/min flowrate. After the pyrolysis, silica was removed by acid treatment in 25 wt% of Hydrofluoric acid (HF) followed by washing with DI water until reaching pH of ~ 6.5 . To further remove unreacted metallic particles, the

powder was treated in 1 M HNO_3 . Additional heat treatment was done in UHP nitrogen atmosphere at 1000°C for 45 min.

2.3 | Physical-chemical characterization

2.3.1 | pH measurement

The pH of the powders was measured on an ink using a pH meter (Thermo Scientific, Orion Versastar Pro), where the ink was prepared with 50 mg catalyst in 10 ml solvent ($\text{H}_2\text{O}/1\text{-propanol}:1/1_{\text{v/v}}$).

2.3.2 | Dynamic light scattering and zeta potential

Dynamic light scattering (DLS) and zeta-potential measurements were carried out using a 90 Plus Pals (Brookhaven). All the measurements were performed at 25°C (50 mg of catalyst 10 ml solvent [$\text{H}_2\text{O}/1\text{-propanol}:1/1_{\text{v/v}}$], diluted 100 times). In the calculation of zeta potential, a Smoluchowski equation was used. Measurements were taken at least three times for the particle size measurement, and at least five times for zeta-potential measurement to ensure repeatability of the results.

2.3.3 | Specific surface area and pore size distribution

The specific surface area and pore size distribution measurements were collected from a N_2 isothermal adsorption experiment by Brunauer–Emmett–Teller (BET, Nova Touch) with DFT model.

2.3.4 | X-ray powder diffraction

Powder diffraction measurements were performed on a Panalytical X'pert Pro instrument with both $\text{Cu K}\alpha$ (1.54 Å) and $\text{Mo K}\alpha$ (0.71 Å) irradiation

2.3.5 | X-ray photoelectron spectroscopy

The photoelectron spectra from the powders were obtained using an ESCALAB Xi+ (Thermo Fisher Scientific) spectrometer utilizing a monochromatic $\text{Al K}\alpha$ source operating at a power of 200 W. The powder samples were placed on double-sided conductive carbon tape before

being introduced into the ultra-high vacuum chamber of the instrument. The survey and high-resolution spectra were acquired at pass energies of 150 and 40 eV, respectively. Due to the adequate electronic conductivity of the samples, it was not necessary to utilize charge neutralization during the measurements. Charge correction was done, where necessary, by shifting the peaks relative to the adventitious C 1s peak at the binding energy of 284.8 eV. All the XPS spectra were fitted using the Advantage (ThermoFisher) software.

2.4 | Ammonia quantification

Ammonia was quantified using a Sequential Injection Analyzer (SIA) system (OmniSIA, FIALab Instruments Inc). For detection and quantification, ammonia is reacted with OPA to make an NH_3 -OPA fluorescent product to be detected with a photomultiplier tube (PMT-FL, FIALab Instruments Inc) with fluorometric detection (excitation at 370 nm and detection at 425 nm). The in-line SIA method uses a peristaltic pump to control the flow of reactants, and an automated two-way valve injects samples into the carrier stream, here the carrier solution was of 0.05 M H_2SO_4 . The sample then mixes with 1 M NaOH (R1) in a mixing coil, shifting the equilibrium from $\text{NH}_4^+(\text{aq})$ to $\text{NH}_3(\text{g})$. Next, the stream flows through a gas diffusion cell with a polypropylene membrane, separating the gaseous ammonia from the liquid stream. The gaseous ammonia diffuses through the membrane into an acceptor stream of OPA solution, which is then passed over a heating coil at 65°C to promote the reactions between NH_3 and OPA-sulfite, forming several fluorescent compounds as described by Kulla and Zuman.⁵⁰ Finally, the stream passes through a flow-through cuvette, where a light source is used to excite fluorescence of the NH_3 -OPA products, and a PMT detects emission. These reactions have different reaction rate constants and the exact composition of fluorescent compounds being measured in the PMT will depend on the conditions of the SIA, most importantly the flow rate and duration of the heating step. For accurate quantification, it is of main importance that the conditions of SIA remain the same throughout the experiment (the reagents, carrier, temperature, and flow rate) so that the calibration curve obtained of ammonia standards holds. Before and after each electrochemical experiment, NH_3 standards are measured in the SIA to obtain a calibration curve, using an autosampler. The calibration standards are matrix matched to the electrolyte and the acid trap, 0.1 M KOH and 0.05 M H_2SO_4 . A linear fit to the calibration curve was used to correlate ammonia concentration to the intensity of the fluorescence emission. A typical calibration curve is shown in Figure S1, in the range 0–0.24 ppm NH_3 in 0.1 M

KOH. The limit of detection was determined as being three times the standard deviation of the lowest concentration measured.²⁶

During electrochemical measurements, samples were measured in-line, using automated syringes, using both gas-tight syringes and PEEK tubing to limit any exposure or handling to air. Samples were collected every 30 min from both directly from the catholyte compartment, and from acid trap as described below. The catholyte gas exhaust was purged through an acid trap to capture concentrate all gaseous ammonia. Before and after experiments, ammonia concentration in the electrolyte and acid trap reservoirs were measured to account for possible drift due to contamination in air or nitrogen gas used. Readers are referred to the Supplementary Material for schematic representation of the experimental setup (Figures S2–S4).

2.5 | Electrochemical measurements

Water-based ink was prepared by mixing the catalyst powder, Vulcan XC 72 carbon black (Fuel Cell Store) and PTFE solution (Fuel Cell Store, PTFE DISP 30) in ratio 85:10:5 by weight and mixed by sonication. The nickel foam was cleaned by sonicating it in 0.5 M HCl and followed by sonication in a 50:50 mixture of ethanol and ultrapure water (MilliQ, Grade 1) and finally sonicated in ultrapure water (MilliQ, Grade 1). The ink was drop-cast onto a 1 cm² nickel foam, the electrode was then dried in a vacuum oven for 12 h at 70°C and pressed in pill press at ~10 MPa pressure to increase adhesion between the active material and the current collector.⁵¹ Finally, the electrode was cleaned with ultrapure water before assembling in the electrochemical cell. The mass loading of catalyst onto the electrode was measured by weighing the electrode before and after drop-casting and is shown in Table 3.

The electrochemical testing was carried out in a 3-electrode H-cell system. The compartments of the working and counter electrodes (WE and CE) were separated by a Nafion™ 211 membrane. The Nafion™ was pretreated to prevent contamination of ammonia from the atmosphere as previously described.³¹ Both electrode chambers were filled with 25 ml of 0.1 M KOH. Saturated Ag/AgCl (Metrohm) was used as a reference electrode. A platinum (Pt) mesh of 1 cm² geometric area connected to a Pt wire was used as the CE. Gas was supplied to the WE compartment at flow rate of 15–20 ml/min after passing through two scrubbing units, a 0.05 M H_2SO_4 acid trap followed by a MQ water trap. Prior to testing, the Ar or N_2 gas was bubbled through the electrolyte for at least 30 min to remove any dissolved gases. The traps prevent residual N-containing species found in the gas from entering the electrolyte. To ensure full analysis of any electrochemically

produced ammonia, the gas outlet from the WE compartment was directed into an acid trap containing 0.45 ml of 0.05 M H_2SO_4 . With a 30 min interval, 1 ml of electrolyte sample and 0.45 ml of acid trap (the complete sample) sample were collected simultaneously for ammonia quantification using automatic syringe pumps, connected to the cell with PEEK tubing. The acid trap sample was first injected for analysis and acid trap volume replaced with fresh acid from a sealed reservoir. Then, the electrolyte sample was injected for analysis, following which the sample volume was replaced to the cathodic chamber with fresh electrolyte from a sealed electrolyte reservoir to maintain 25 ml electrolyte volume. The H-cell was connected to Gamry 600E potentiostat (Gamry Instruments). Unless otherwise stated, the specific current was normalized to the catalyst mass loading. The pH of the electrolyte solution was measured before and after electrochemical testing and was in the range 13.2–13.6.

Each electrode/gas combination was characterized by performing the following electrochemical techniques in the same order: Open circuit potential (OCP) was measured until stabilization. Then, the surfaces went through a series of priming steps, where cyclic voltammetry (CV) scans were performed toward reducing potentials. Linear sweep voltammetry (LSV) at 10 mV/s was then used to probe the onset potential (OP) determined when specific current reached 1 mA/mg. Tafel slopes were calculated from the linear region of the $\log(i)$ versus RHE between -0.2 and -0.3 V versus RHE. The double-layer capacitance was probed for each catalyst by performing CV scans in the non-Faradic region, increasing the scan rate from 5 to 100 mV/s. Potentiostatic electrochemical impedance spectroscopy was performed, using 10 mV voltage perturbation at the Faradaic potential in the frequency range 0.1 MHz–0.1 Hz with 10 points per decade.

To study electrocatalysis, pulsed loop chronoamperometry studies were applied for 30 min for each set of chosen potentials, a methodology developed in our previous work on NRR catalysis.²⁸ A potential close to OCP is chosen as an adsorption potential (A) at which the system can equilibrate and allow for adsorption of nitrogen molecules to the surface. The “catalysis potentials” (C) were selected close to the OP of HER based on the LSV scans and pulsed against the OCP (10 s reduction and 50 s OCP, for system relaxation and nitrogen adsorption). This pattern was repeated for 28 loops, and in between each chronoamperometry loops, three CV cycles were collected to probe the stability of the electrode. Thus, each cycle amounts to 30 min, after which samples of electrolyte and acid trap were collected automatically for quantification of ammonia, as described above. Three values of A were examined (OCP, OCP+200 mV, and OCP+400 mV) and three values of C around the OP (± 200 mV).

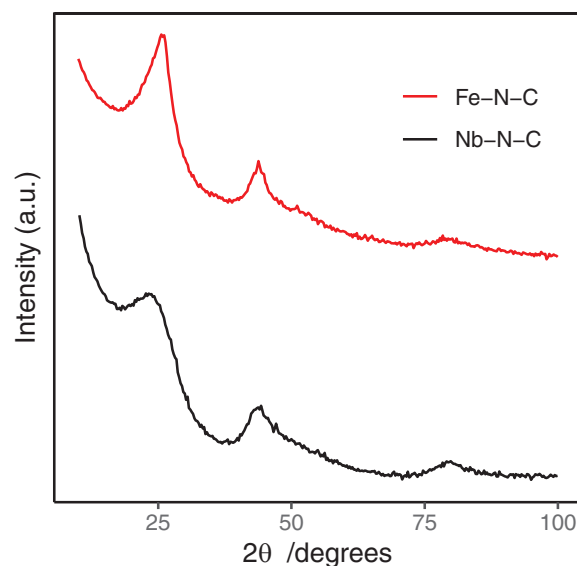


FIGURE 1 XRD diffractogram of Fe-N-C and Nb-N-C electrocatalysts collected with Cu $K\alpha$ irradiation

3 | RESULTS AND DISCUSSION

As synthesized, electrocatalysts were characterized by X-ray diffraction (XRD), X-ray photoelectron spectroscopy (XPS), nitrogen isotherm pore size analysis, DLS particle size method, zeta potential, and thermogravimetric analysis. The material characterization is summarized in Table 1.

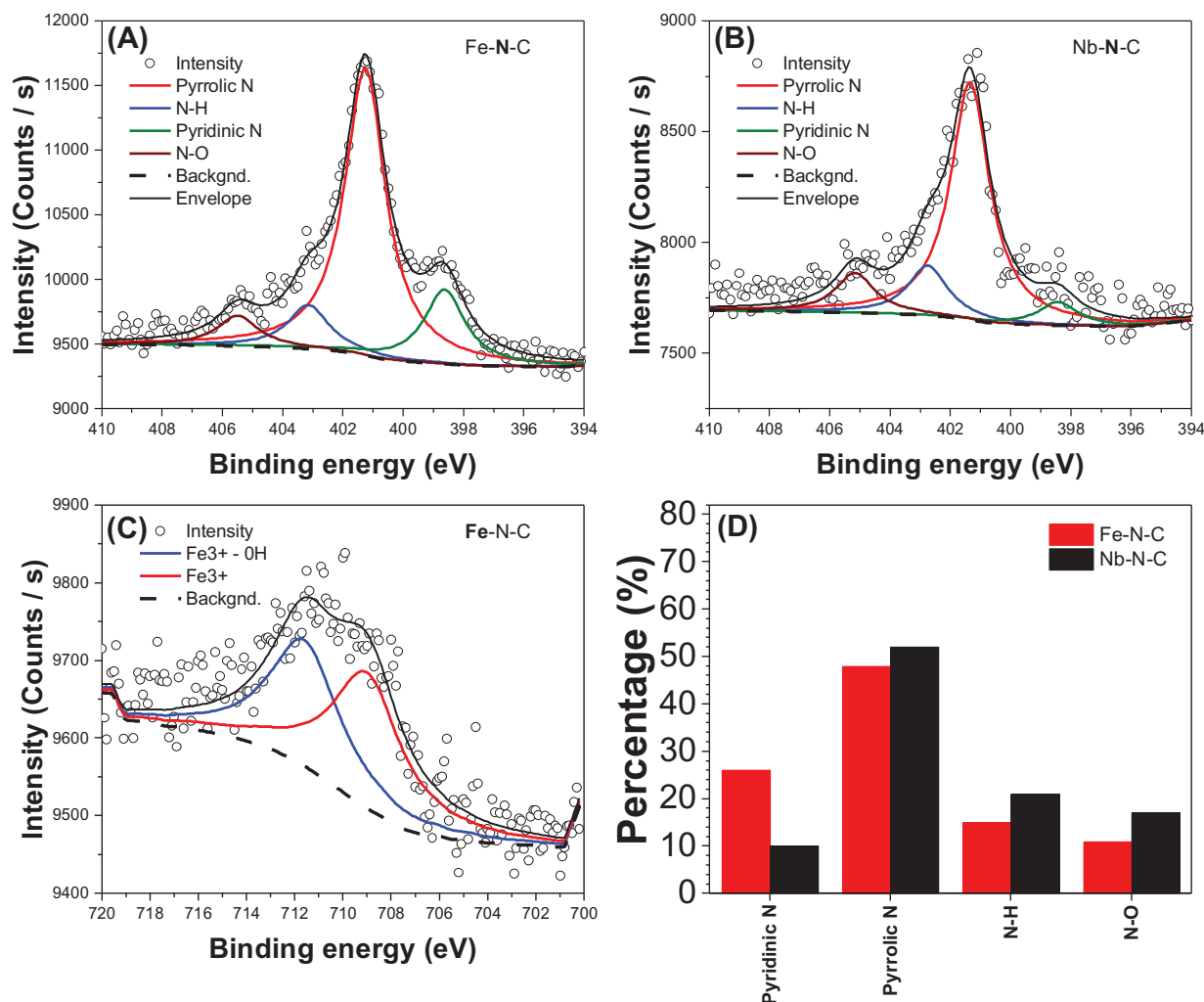
The XRD powder patterns (Figure 1) show the typical carbon-related peaks, a broad peak around $2\theta = 25^\circ$, attributed to the carbon (002) plane, at 45° (100) and 79° (110). No metallic Fe and Fe_3C is observed in Fe-N-C catalyst (also measured with Mo $K\alpha$ source, Figure S5) demonstrating that the washing with both HF and HNO_3 after synthesis effectively removed these phases. Only iron phases covered with thick layers of graphite can in principle exist after such treatment but are not observed.

Analysis of surface area and pore size distribution shows that these materials possess high surface area with values above $1000 \text{ m}^2 \text{ g}^{-1}$ (Table 1). The high surface area derives from using silica as a template, as well as vigorous decomposition of organic precursors and the removal of unreacted metallic phases (mainly oxides, carbides, and nitrides) with HNO_3 acid after synthesis. The Nb-N-C sample has a smaller pore size, in the range of 5–9 nm compared to 9–13 nm for Fe-N-C. It is expected that smaller pores will increase the retention time of N_2 at the surface, increasing its probability to adsorb on an active site.

The primary particle size distribution of materials made by hard template method can be indication of accessibility of active centers by reagents. However, it has been shown that such catalysts consist of highly developed internal

TABLE 1 Morphological characterization and surface properties of electrocatalysts

Sample	Surface area/ $\text{m}^2 \text{g}^{-1}$	Particle size distribution (DLS)/nm	Carbon domain size (XRD)/nm	Zeta potential (mV)	Immersed pH
Fe-N-C	1110	488 ± 14	1.1	32 ± 5	5.7
Nb-N-C	1038	464 ± 21	1.4	24 ± 5	5.9

**FIGURE 2** The N 1s detailed XPS spectra from the catalyst powders (A) Fe-N-C and (B) Nb-N-C with the corresponding (C) Fe 2p spectrum from the Fe-N-C. (D) The relative N species per catalyst

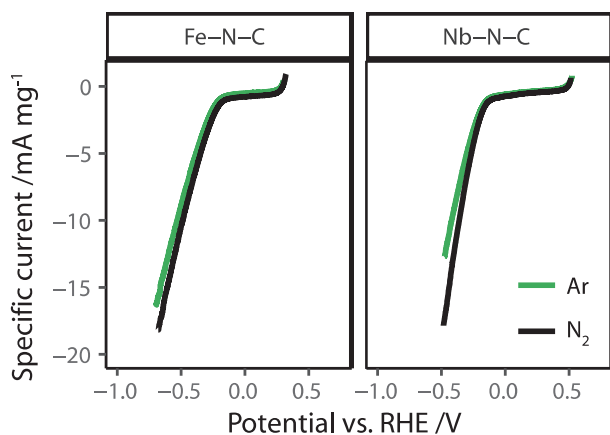
network of pores, which require smaller primary particles for better access to the active sites.³⁹ Based on the results of DLS, the carbon particles (which include not only primary particles but also aggregates and agglomerates) were close to 500 nm, which in a combination with pore sizes in the range 5–13 nm gives an instant access to the active sites located in the porous matrix of these particles. The pH of the powders was slightly acidic, indicating that these materials are prone to protonation—a property that could positively enhance NRR, for the adsorbed nitrogen to be protonated to NH_3 , or for the same reasoning, promote HER (Table 1). Furthermore, the high value of

zeta potential shows that these particles should form a stable colloidal solution, an important property for large-scale manufacture of, that is, gas diffusion electrodes.

The XPS N 1s spectra of Fe-N-C and Nb-N-C (Figure 2A,B) show the different types of nitrogen environments and its relative concentrations (Figure 2D). The two catalysts consist of pyrrolic N (401.3 eV), pyridinic N (398.5 eV), N-O (405.2 eV), and N-H (≈ 403 eV). The pyrrolic N is most prominent (Figure 2D) for both catalysts. The metal components of the catalysts have very low photoelectron signals due to the low content of these shown, specifically the Fe $2p_{3/2}$ spectrum for

TABLE 2 Chemical composition of Fe-N-C and Nb-N-C according to XPS results

Sample	N, at%	C, at%	O, at%	Metal (Fe, Nb), at%
Fe-N-C	3.3	92.6	4.1	≤0.1
Nb-N-C	2.7	95.7	1.6	≤0.1

**FIGURE 3** Linear sweep voltammetry (LSV) for Fe-N-C and Nb-N-C in Ar-saturated (green) and N₂-saturated (black) electrolyte

the Fe-N-C catalyst is shown in Figure 2C. The Nb 3d spectrum showed no peaks, indicating negligible amount of Nb or too low (< 0.1 at.%) to be measured via XPS. The Fe 2p spectrum indicates that there are two peaks at BEs of 709.0 and 711.6 eV that can be attributed to Fe³⁺ and Fe³⁺ bound to OH⁻, respectively, indicating oxidized Fe species on the surface.⁵² The overall chemical composition is summarized in Table 2.

Electrochemical characterization of the electrode materials was performed in both Ar and N₂ environments to probe the activity toward NRR. The gas, either Ar or N₂, after passing through scrubbing units was constantly purged through the electrolyte to ensure saturation in the electrolyte. First, the OCP was recorded for 20 min prior to passing any current. The OCP value was taken as the upper limit potential in all further studies, to avoid any oxidation of the surface. LSV profiles were collected at 10 mV/s, from OCP toward more negative potentials, as shown in Figure 3. The OP, attributed to the HER reaction, is similar for both electrodes, -0.11 and -0.15 V versus RHE in N₂ (Fe-N-C and Nb-N-C, respectively) and -0.14 and -0.20 V

versus RHE in Ar (Fe-N-C and Nb-N-C, respectively), suggesting a slight shift to less negative potentials in the N₂ environment (Table 3). The Tafel slopes, however, calculated from the LSV curves are around 100 mV/dec for both surfaces and gases.

The double-layer capacitance was estimated by recording cyclic voltammograms (CVs) at different scan rates from 5 to 100 mV/s in the capacitive region, away from Faradaic potentials shown for Fe-N-C in Figure 4A,B (and Nb-N-C in Figures S8 and S9).

The specific capacitance was calculated from the linear slope of the maximum specific current (Figure 4C), summarized in Table 3. Interestingly, the specific capacitance is higher in the N₂ environment for both Fe-N-C and Nb-N-C, suggesting an effect of N₂ on the electric double layer. This effect is the subject of further investigation.

To investigate the catalytic activity of these materials toward NRR, chronoamperometry loops were applied where the H-cell was connected to an automated, in-line SIA quantification unit. The quantification system allows for direct analysis of ammonia during electrochemistry, which mitigates both possible NH₃ losses and external sources contamination in the measured samples. Figure 5 shows the reaction rate calculated based on the quantified NH₃ for Fe-N-C catalyst—no statistically relevant ammonia production was observed in these tests as indicated by the significant error bars and calculated current efficiency below 0.1%. Similar results were obtained for Nb-N-C (Figure S7), demonstrating that these materials are not active under the reaction environment provided in this study. However, the subject of future studies is to increase the access to N₂ gas at catalytic sites and overcome the low solubility of nitrogen in aqueous solutions by using gas diffusion electrodes. Li et al. demonstrated an increase in reaction rate on Fe-based SAC catalyst using gas diffusion electrode in a flow cell compared to H-cell (from 3 nmol g⁻¹ s⁻¹ to 0.01 mmol g⁻¹ s⁻¹).⁴⁸

TABLE 3 The onset potential (OP), Tafel slopes calculated from the LSV profiles in Figure 2, between -0.2 and -0.3 V versus RHE and the specific capacitance calculated from Figure 3 in Ar and N₂ for the three different electrode surfaces

Gas medium	Fe-N-C				Nb-N-C			
	OP (V vs. RHE)	Tafel slope (mV/dec)	Specific capacitance (mF/mg)	Mass loading (mg)	OP (V vs. RHE)	Tafel slope (mV/dec)	Specific capacitance (mF/mg)	Mass loading (mg)
Ar	-0.20	97	34	3.0	-0.14	104	29	2.6
N ₂	-0.15	104	53	4.1	-0.11	100	42	2.3

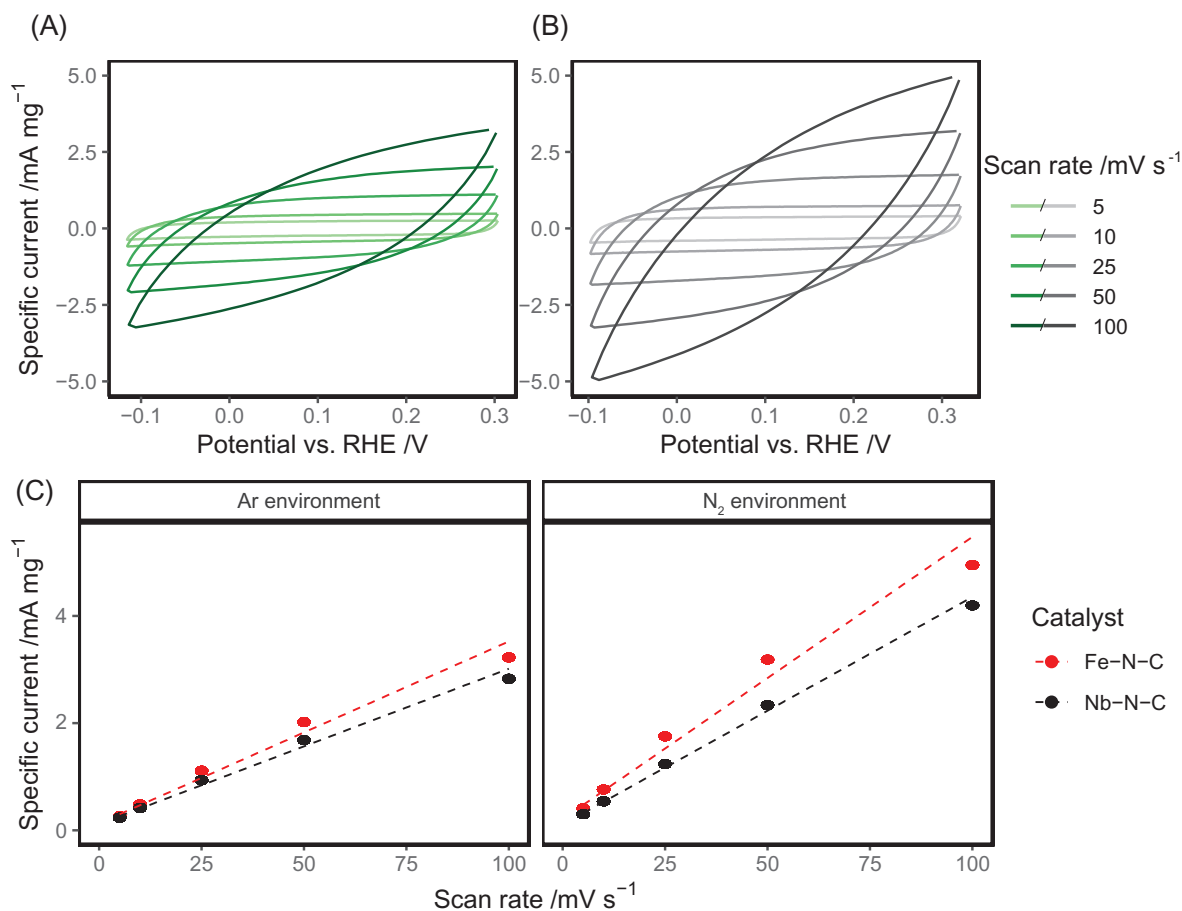


FIGURE 4 Cyclic voltammetry scans on Fe-N-C at different scan rates in (A) Ar and (B) N₂ environment. (C) Linear best fit to the CV scan rate study for Fe-N-C and Nb-N-C in Ar and N₂ gas environment

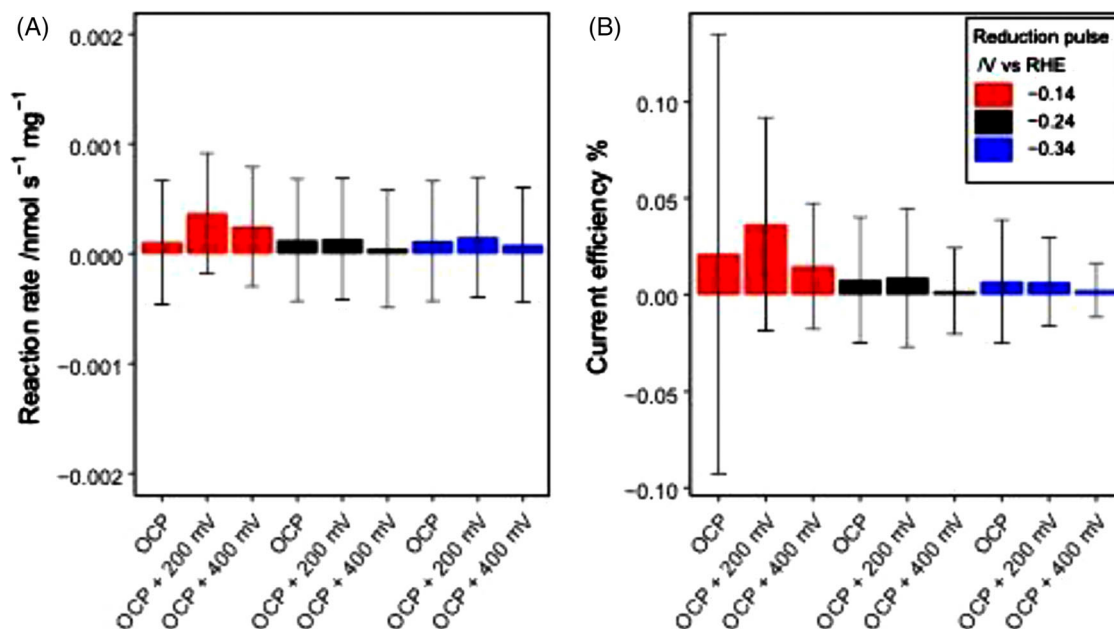


FIGURE 5 (A) The reaction rate nmol mg⁻¹ s⁻¹ for NRR on Fe-N-C calculated based on the quantified ammonia during chronoamperometric loops. The labels indicate the potential during the adsorption potential (A, see experimental details), and colors indicate potential during the reduction pulse (C) and (B) the corresponding current efficiency

4 | CONCLUSIONS

We conclude that the Fe-N-C and Nb-N-C electrocatalysts are not active for NRR within the electrochemical setup in this work (using an H-cell in alkaline media). The electrochemical analysis data demonstrate slightly earlier onset for Faradaic reactions, resulting in increased current density in LSV records in N₂, as well as a significantly greater capacitance in N₂ for both Fe-N-C and Nb-N-C, when compared with Ar environment. This suggests an effect of nitrogen at the catalyst surface but the metal centers in this case (Fe and Nb) do not catalyze its reduction. Furthermore, we demonstrate a robust experimental NRR methodology with an in-line SIA ammonia quantification. The method is automated, where 200 μ l volume of electrolyte is sampled in gas-tight tubing every 5–10 min, which prevents human errors or exposure of the samples to the environment showing the possibility of obtaining a reproducible negative result. The results can be synchronized with the electrochemistry and trends observed over time, which allows for thorough and high-throughput screening of potential NRR electrocatalysts. Considering detailed description of the procedure, availability of materials and instruments, the proposed method can be recommended for use by researchers working in the field of NRR to produce reproducible results free of false-positive measurements of ammonia.

ACKNOWLEDGMENTS

Atmonia and the University of Iceland would like to acknowledge the Icelandic Research Fund (grant 196437-051) and the Icelandic Technology Development Fund (grant 175350-0611) for the financial support of this work. ABG gratefully acknowledges financial support from the Icelandic Research Fund (grant 1515–1513377). AS and BZ gratefully acknowledge the financial support from the U.S. Department of Energy's Office of Energy Efficiency and Renewable Energy (EERE) under the Hydrogen and Fuel Cells Technologies Office (HFTO), FY2018 Hydrogen and Fuel Cell R&D FOA, Award Number DE-EE0008419, and support from Companhia Brasileira de Metalurgia e Mineração (CBMM).

CONFLICT OF INTEREST

The authors declare no conflict of interest.

DISCLAIMER

This manuscript has been authored by UT-Battelle, LLC, under contract DE-AC05-00OR22725 with the U.S. Department of Energy (DOE). The U.S. government retains and the publisher, by accepting the article for publication,

acknowledges that the U.S. government retains a nonexclusive, paid-up, irrevocable, worldwide license to publish or reproduce the published form of this manuscript, or allow others to do so, for U.S. government purposes. DOE will provide public access to these results of federally sponsored research in accordance with the DOE Public Access Plan (<http://energy.gov/downloads/doe-public-access-plan>).

ORCID

Charl J. Jafta  <https://orcid.org/0000-0002-9773-6799>

Alexey Serov  <https://orcid.org/0000-0003-3182-4726>

REFERENCES

1. Lan R, Irvine JT, Tao S. Ammonia and related chemicals as potential indirect hydrogen storage materials. *Int J Hydrog Energy*. 2012;37(2):1482-1494.
2. Liu H, Fu C, Gu T, et al. Corrosion behavior of carbon steel in the presence of sulfate reducing bacteria and iron oxidizing bacteria cultured in oilfield produced water. *Corros Sci*. 2015;100:484-495.
3. Deng J, Iñiguez JA, Liu C. Electrocatalytic nitrogen reduction at low temperature. *Joule*. 2018;2(5):846-856.
4. Smil V. *Fritz Haber, Carl Bosch, and the Transformation of World Food Production*. MIT Press; 2001.
5. Blok K. *Efficient Use and Conservation of Energy*. Eolss Publishers; 2009.
6. Norskov J, Chen J, Bullock M, Chirik P, Chorkendorff I. Sustainable Ammonia Synthesis. DOE Roundtable Report. 2016.
7. Wan Y, Xu J, Lv R. Heterogeneous electrocatalysts design for nitrogen reduction reaction under ambient conditions. *Mater Today*. 2019;27:69-90.
8. Van der Ham CJ, Koper MT, Hetterscheid DG. Challenges in reduction of dinitrogen by proton and electron transfer. *Chem Soc Rev*. 2014;43(15):5183-5191.
9. John J, Lee D-K, Sim U. Photocatalytic and electrocatalytic approaches towards atmospheric nitrogen reduction to ammonia under ambient conditions. *Nano Conver*. 2019;6(1):1-16.
10. Kyriakou V, Garagounis I, Vourros A, Vasileiou E, Stoukides M. An electrochemical Haber-Bosch process. *Joule*. 2020;4(1):142-158.
11. Nash J, Yang X, Anibal J, Wang J, Yan Y, Xu B. Electrochemical nitrogen reduction reaction on noble metal catalysts in proton and hydroxide exchange membrane electrolyzers. *J Electrochem Soc*. 2017;164(14):F1712.
12. Cui X, Tang C, Zhang Q. A review of electrocatalytic reduction of dinitrogen to ammonia under ambient conditions. *Adv Energy Mater*. 2018;8(22):1800369.
13. Guo R, Hu M, Zhang W, He J. Boosting electrochemical nitrogen reduction performance over binuclear Mo atoms on N-doped nanoporous graphene: a theoretical investigation. *Molecules*. 2019;24(9):1777.
14. Song P, Wang H, Kang L, Ran B, Song H, Wang R. Electrochemical nitrogen reduction to ammonia at ambient conditions on nitrogen and phosphorus co-doped porous carbon. *Chem Commun*. 2019;55(5):687-690.
15. Skulason E, Bligaard T, Gudmundsdóttir S, et al. A theoretical evaluation of possible transition metal electro-catalysts for N₂ reduction. *Phys Chem Chem Phys*. 2012;14(3):1235-1245.

16. Singh AR, Rohr BA, Statt MJ, Schwalbe JA, Cargnello M, Nørskov JK. Strategies toward selective electrochemical ammonia synthesis. *ACS Catal.* 2019;9(9):8316-8324.
17. Singh AR, Rohr BA, Schwalbe JA, et al. *Electrochemical Ammonia Synthesis—The Selectivity Challenge*. ACS Publications; 2017.
18. Andersen SZ, Čolić V, Yang S, et al. A rigorous electrochemical ammonia synthesis protocol with quantitative isotope measurements. *Nature.* 2019;570(7762):504-508.
19. Lazouski N, Chung M, Williams K, Gala ML, Manthiram K. Non-aqueous gas diffusion electrodes for rapid ammonia synthesis from nitrogen and water-splitting-derived hydrogen. *Nat Catal.* 2020;3(5):463-469.
20. Choi J, Suryanto BH, Wang D, et al. Identification and elimination of false positives in electrochemical nitrogen reduction studies. *Nat Commun.* 2020;11(1):1-10.
21. Krug F, Růžička J, Hansen E. Determination of ammonia in low concentrations with Nessler's reagent by flow injection analysis. *Analyst.* 1979;104(1234):47-54.
22. Searle PL. The Berthelot or indophenol reaction and its use in the analytical chemistry of nitrogen. A review. *Analyst.* 1984;109(5):549-568.
23. Iriawan H, Andersen SZ, Zhang X, et al. Methods for nitrogen activation by reduction and oxidation. *Nat Rev Methods Primers.* 2021;1(1):1-26.
24. Shipman MA, Symes MD. A re-evaluation of Sn (II) phthalocyanine as a catalyst for the electrosynthesis of ammonia. *Electrochim Acta.* 2017;258:618-622.
25. Greenlee LF, Renner JN, Foster SL. The use of controls for consistent and accurate measurements of electrocatalytic ammonia synthesis from dinitrogen. *ACS Catal.* 2018;8(9):7820-7827.
26. Kibsgaard J, Nørskov JK, Chorkendorff I. The difficulty of proving electrochemical ammonia synthesis. *ACS Energy Lett.* 2019;4(12):2986-2988.
27. Li L, Tang C, Yao D, Zheng Y, Qiao S-Z. Electrochemical nitrogen reduction: identification and elimination of contamination in electrolyte. *ACS Energy Lett.* 2019;4(9):2111-2116.
28. Hanifpour F, Canales CP, Fridriksson EG, et al. Investigation into the mechanism of electrochemical nitrogen reduction reaction to ammonia using niobium oxynitride thin-film catalysts. *Electrochim Acta.* 2022;403:139551.
29. Aminot A, Kérouel R, Birot D. A flow injection-fluorometric method for the determination of ammonium in fresh and saline waters with a view to in situ analyses. *Water Res.* 2001;35(7):1777-1785.
30. Watson RJ, Butler EC, Clementson LA, Berry KM. Flow-injection analysis with fluorescence detection for the determination of trace levels of ammonium in seawater. *J Environ Monit.* 2005;7(1):37-42.
31. Hanifpour F, Sveinbjörnsson A, Canales CP, Skúlason E, Flosadóttir HD. Preparation of nafion membranes for reproducible ammonia quantification in nitrogen reduction reaction experiments. *Angew Chem.* 2020;132(51):23138-23142.
32. Kaiser SK, Chen Z, Faust Akl D, Mitchell S, Perez-Ramirez J. Single-atom catalysts across the periodic table. *Chem Rev.* 2020;120(21):11703-11809.
33. Gokhale R, Chen Y, Serov A, Artyushkova K, Atanassov P. Novel dual templating approach for preparation of highly active Fe-NC electrocatalyst for oxygen reduction. *Electrochim Acta.* 2017;224:49-55.
34. Osmieri L, Escudero-Cid R, Armandi M, et al. Fe-N/C catalysts for oxygen reduction reaction supported on different carbonaceous materials. Performance in acidic and alkaline direct alcohol fuel cells. *Appl Catal, B.* 2017;205:637-653.
35. Gokhale R, Asset T, Qian G, et al. Implementing PGM-free electrocatalysts in high-temperature polymer electrolyte membrane fuel cells. *Electrochem Commun.* 2018;93:91-94.
36. Li M, Wang H, Luo W, Sherrell PC, Chen J, Yang J. Heterogeneous single-atom catalysts for electrochemical CO₂ reduction reaction. *Adv Mater.* 2020;32(34):2001848.
37. Lü F, Bao H, Mi Y, et al. Electrochemical CO₂ reduction: from nanoclusters to single atom catalysts. *Sustain Energy Fuels.* 2020;4(3):1012-1028.
38. Gao D, Liu T, Wang G, Bao X. Structure sensitivity in single-atom catalysis toward CO₂ electroreduction. *ACS Energy Lett.* 2021;6(2):713-727.
39. Serov A, Artyushkova K, Niangar E, et al. Nano-structured non-platinum catalysts for automotive fuel cell application. *Nano Energy.* 2015;16:293-300.
40. Thompson ST, Wilson AR, Zelenay P, et al. ElectroCat: DOE's approach to PGM-free catalyst and electrode R&D. *Solid State Ionics.* 2018;319:68-76.
41. Vecchio CL, Serov A, Romero H, et al. Commercial platinum group metal-free cathodic electrocatalysts for highly performed direct methanol fuel cell applications. *J Power Sources.* 2019;437:226948.
42. Adabi H, Shakouri A, Ul Hassan N, et al. High-performing commercial Fe-N-C cathode electrocatalyst for anion-exchange membrane fuel cells. *Nat Energy.* 2021;6(8):834-843.
43. Akula S, Mooste M, Zulevi B, et al. Mesoporous textured Fe-NC electrocatalysts as highly efficient cathodes for proton exchange membrane fuel cells. *J Power Sources.* 2022;520:230819.
44. Roy A, Hursán D, Artyushkova K, Atanassov P, Janáky C, Serov A. Nanostructured metal-NC electrocatalysts for CO₂ reduction and hydrogen evolution reactions. *Appl Catal, B.* 2018;232:512-520.
45. Xiang Z, Li L, Wang Y, Song Y. Recent advances in noble-metal-free catalysts for electrocatalytic synthesis of ammonia under ambient conditions. *Chemistry.* 2020;15(12):1791-1807.
46. Choi C, Back S, Kim N-Y, Lim J, Kim Y-H, Jung Y. Suppression of hydrogen evolution reaction in electrochemical N₂ reduction using single-atom catalysts: a computational guideline. *ACS Catal.* 2018;8(8):7517-7525.
47. Niu H, Wang X, Shao C, Zhang Z, Guo Y. Computational screening single-atom catalysts supported on g-CN for N₂ reduction: high activity and selectivity. *ACS Sustain Chem Eng.* 2020;8(36):13749-13758.
48. Li J, Chen S, Quan F, et al. Accelerated dinitrogen electroreduction to ammonia via interfacial polarization triggered by single-atom protrusions. *Chem.* 2020;6(4):885-901.
49. Kishi H, Sakamoto T, Asazawa K, et al. Structure of active sites of Fe-NC nano-catalysts for alkaline exchange membrane fuel cells. *Nanomaterials.* 2018;8(12):965.
50. Kulla E, Zuman P. Reactions of orthophthalaldehyde with ammonia and 2-aminoethanol. *Org Biomol Chem.* 2008;6(20):3771-3780.
51. Liu H-H, Zhang H-L, Xu H-B, Lou T-P, Sui Z-T, Zhang Y. Hierarchically nanostructured vanadium nitride microspheres assembled with porous nanosheets fabricated by a template-free route. *Ceram Int.* 2018;44(2):1583-1588.

52. Arrigo R, Schuster ME. On the high structural heterogeneity of Fe-impregnated graphitic-carbon catalysts from Fe nitrate precursor. *Catalysts*. 2019;9(4):303.

SUPPORTING INFORMATION

Additional supporting information can be found online in the Supporting Information section at the end of this article.

How to cite this article: Sveinbjörnsson A, Gunnarsdóttir AB, Creel EB, et al. Demonstration of no catalytical activity of Fe-N-C and Nb-N-C electrocatalysts toward nitrogen reduction using in-line quantification. *SusMat*. 2022;2:476–486. <https://doi.org/10.1002/sus2.81>